sciendo

DOI: 10.2478/rjti-2022-0014

ROMANIAN JOURNAL
OF TRANSPORT INFRASTRUCTURE

SLOPE STABILIZATION OF TWIN-TUBES TUNNEL PORTAL BY ANCHOR BOLTS SUPPORT SYSTEM

Houssam Khelalfa, Civil Engineering and Environment Laboratory (LGCE) of University of Jijel, Jijel, Algeria; Faculty of Engineering and Technology, Selinus University of Science and Literature (SUSL), Bologna , Italy
U. Sakalli, MAPA İNŞAAT AŞ, Ankara, Turkey
E. B. Aygar, MAPA İNŞAAT AŞ, Ankara, Turkey
O.Şimşek, MAPA İNŞAAT AŞ, Ankara, Turkey
Bünyamin Aykan, MAPA İNŞAAT AŞ, Ankara, Turkey
H. Boulmaali, MAPA İNŞAAT AŞ, Ankara, Turkey

Abstract

It is not known in the literature why the behavior of rocks incurs the tunnel excavation and it remains unclear for what has been calculated in the initial studies. That's why the most important thing to consider in tunnel construction works is to monitor rock mass behavior. The finite element method (FEM) can also analytically represent the static and dynamic behavior of the rock mass. Concretely, this makes it possible to calculate the behavior of very complex objects numerically. The present study embraces a geophysical prospecting which was carried out by the method of surface seismic tomography to reveal the lithology of the different formations and their geometry and the variation in speed of the subsurface formations at the level of the South portal of the Texana tunnel on Jijel province, in Algeria. The paper also consists in making a two-dimensional numerical study of the stability of the tunnel portals with the Phase.2 2D program. On the other hand, the calculation results will be compared with in-situ surveying to strengthen the numerical modeling. It can be concluded that the Anchor Bolts Support System gives good results in terms of displacement of the rock mass and satisfactory stability in terms of collapse analyzis of the tunnel portals.

Keywords: Geophysical Survey, rock masses of flysch , Collapse, Anchor Bolts, Numerical Modeling, Displacement Control.

1 INTRODUCTION

The underground structures such as tunnels are very complex to build, because their actual behavior often differs in varying proportions from the behavior expected during the initial design stages [1-2]. This discrepancy is due to the fact that many uncertainties are involved in both the variable geological properties and the complex geomechanical properties of rock masses, especially of poor quality [3-7], as well as in the high initial stresses that affect them [8 -15]. However, in tunneling, there is no specific procedure to assess the behavior of the rock mass during digging with respect to the failure mechanism previously defined in the design process [16-18]. Hence, the stability of portal slopes should not be considered separately from tunneling [19-21], because the collapse that may occur during the excavation of the portal will completely stop the tunnel digging [22- 27]. Thus, practical limitations greatly affect the ability to assess the stability of rock sections and slopes in real time, so we use analytical methods such as kinematics, LE, FE or discrete element modeling [28-31]. Experimental and numerical design approaches are very important in the viable and efficient design of support systems and in the analysis of the stability of tunnels and underground excavations [32-35]. The 2D and 3D finite element method was used to analyze the behavior of the rock mass, the in situ stresses and redistribution, the plastic thickness around the tunnel and the performance of the design trusses in order to compare the results of the calculations with the field monitoring to validate the numerical models [36-39]. Therefore, surface displacement measurements and their observation in portal sections is a critical issue in the design of tunneling projects [40-41]. To bridge the gap between measured and expected behaviors, there is a monitoring procedure, which is an integrated design approach to constructing ground structures [42]. Accordingly, the performance of structures is monitored by field measurements, and displacement is usually measured during construction. In addition, the original design can be validated and, if necessary, the original design can be modified [43], as implemented in several projects [44-50].



Figure 1. Satellite Images of the Project Area (ref. Google earth-36°39'48.28" N, 5°45'46.82"E): UTM coordinates: (X = 748 260 Y = 4 060 000); (X = 748 420 Y = 4 059 880).

The study site for the Texana Tunnel project - Jijel – El Eulma highway penetrating at the south portal, is located about 1.5 km southeast of downtown Texana (figure 1). The study area is located at the southern limit of the Petite Kabylie massifs; it spreads across a major geodynamic limit of northern Algeria. Geologically speaking, this limit is associated with several strongly tectonized structural units framed by the largest tectonic contacts of Alpine age in northern Algeria. These contacts are at the origin of the formation of the Maghrebian orogen [51]. The building of the latter results from the structuring of the Maghreb basin and its margins, a basin which was located between the European and African continental margins [52]. The South Kabyle accident (South Kabyle backbone) is considered as the major geodynamic limit of northern Algeria. The geological conditions of the Texana Tunnel site are composed of the Mauritanian Flysh, which are essentially formed of alternations of sandstone and sandstone with passages of hard quartzite, resting on fractured and weathered schists at the surface [53]. All of these formations cover the formation of hard argillite (clay-

stone) which is little altered and fractured and whose upper part and depth are very hard and little fractured. This argillite is present almost all along the tunnel. The prospected terrain, at the level of the south portal, presents a relatively bumpy topography, with fairly pronounced slopes (figure 2).

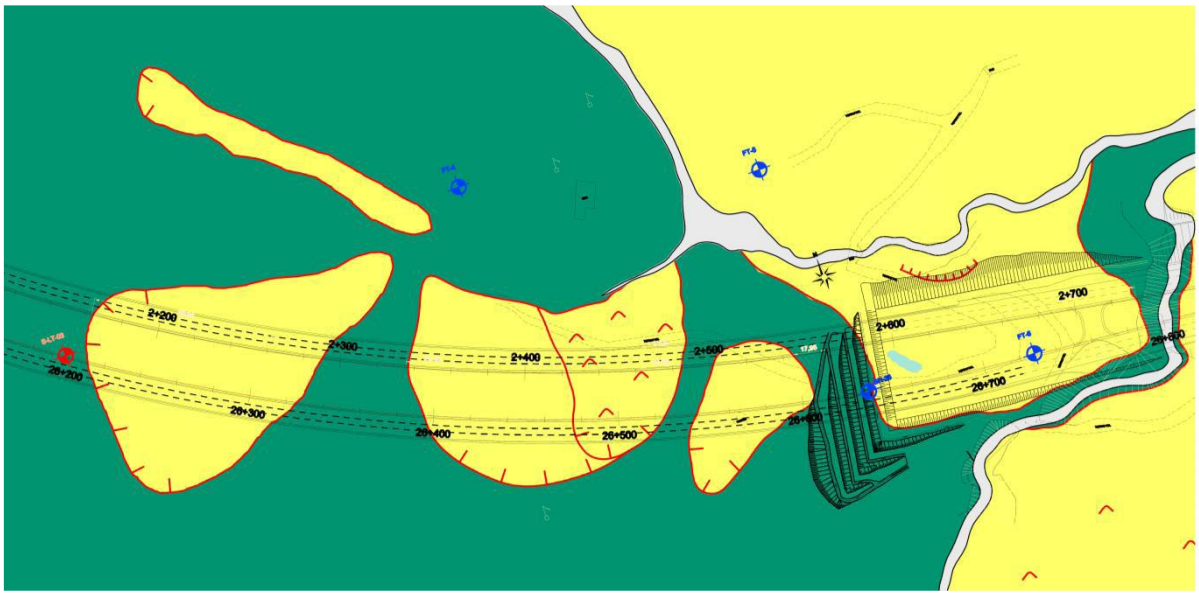

Figure 2. Installation plan of the borehole located on the South Portal section of the tunnel located on an extract from the geological map of Tamesguida, (scale 1/50,000).

2 GEOLOGY AND THE GEOTECHNICAL CONDITION OF THE SOUTH SIDE (SOUTH PORTAL) OF THE TUNNEL

The south portal is located to the south of the route in the flysch unit (Figure 3), in the northeast part of an elongated hill approximately in a southeasterly direction. The two small rivers flowing north and south of the portal show that the groundwater has a high level. In this section the fresh broken color of flysch is dark gray, the decay color is yellowish brown, fine-medium stratified, well-foliated, medium decayed mudstone and thin granular sandstone in low rock feature. The foliations in the mudstone units is well developed. The foliations are parallel to the surfaces of the stratum and the average inclination varies between 70 to 85°. Three soundings were made in the south portal. The FT-4 and FT-5 surveys are located in the eastern slope of the portal. Although the place where the boreholes were opened had the same properties of the rock, it was not located on the portal. According to the soundings it was seen that the first 10 meters of

the surface of the flysch unit is very decomposed and has low rock functionality and decomposition is decreased, and the resistance is increased to medium-strong progressed to deep. In the FT-6 survey (sounding) which is approximately 120 meter southeast of the south portal, the first 18 meter chaotic landslide material was cut.



Figure 3: The general pathway of the south portal and the shallow landslide that is developed on the slope inclined to the north.

Beneath this unit, the low-medium decomposed flysch unit and low rock feature have been cut. This material is the material carried by an old landslide which is caused by the slope to the south of the south portal and there is no portal stability effect. The landslide mass is on the red elevation and it will be cleaned by scraping during road construction. It was seen from the shallow streams to the west and east slope of the hill where the south portal is located (Figure 4).



Figure 4: The south portal and a shallow landslide west of the portal.

In places where there are streams, it has been seen that old trees are tilted and that some of these trees are dead (Figure 5). In addition, some bare places show that around this place there are current landslides and because of this landslide the forest cover cannot be developed. During the excavation of the portal there should be scraped the shallow flows which are mapped on the south portal.



Figure 5: On the tunnel route and at the place near the south portal outcropping in dark gray-beige color, fine-medium stratified and foliated mudstones.

3 GEOPHYSICAL STUDY OF THE SOUTH PORTAL OF THE TEXANA TUNNEL

In addition to the profile obtained at the conclusion of the geological mapping and survey studies carried out in the field, the geophysical studies has also been evaluated (figure 6) and the geological plan and profile are presented below. Following the geophysical work carried out using the seismic-refraction method in the South exit portal, the data from the FT-6 survey and the terrain mapping work were revised and the thickness of the terrain was estimated at approximately 16 m.

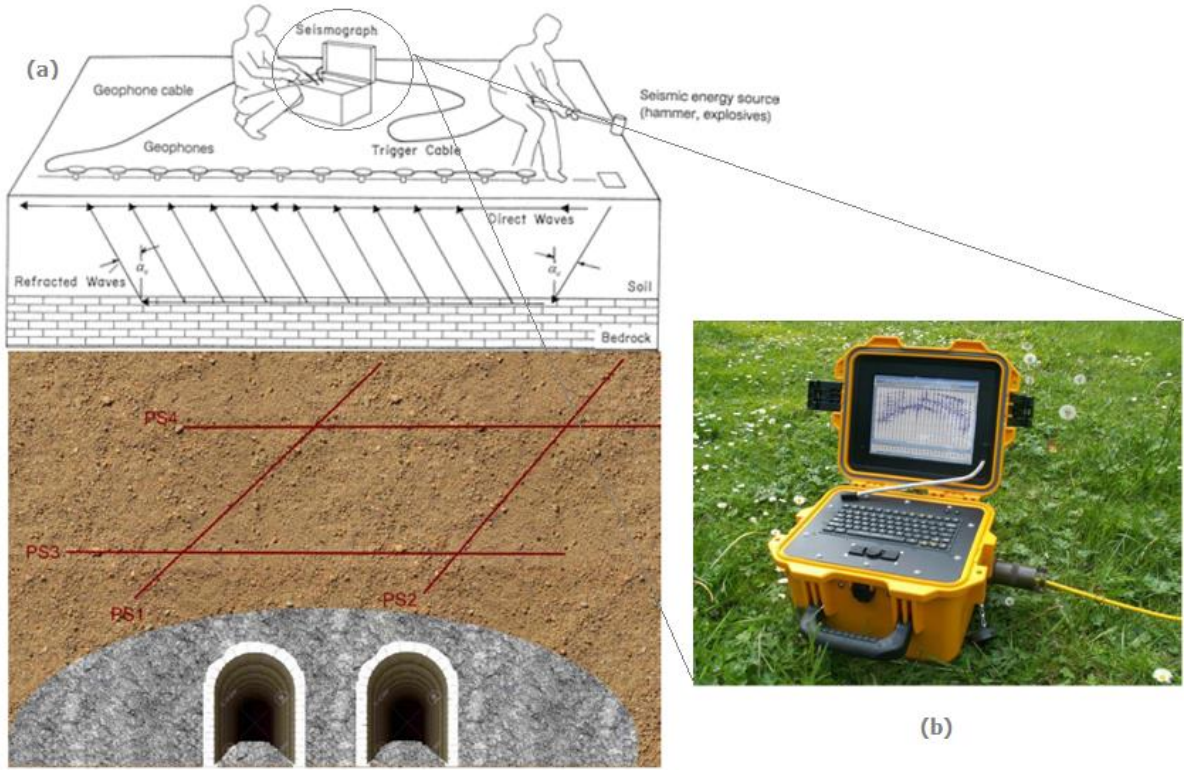

Figure 6. Data acquisition: **(a)** The equipment made available for this study is listed in the following: A seismograph for seismic acquisition - the SUMMIT X STREAM Pro from DMT – Germany, equipped with the following accessories; Two seismic cables with 12 outputs each (take out) spaced 5 meters apart, A seismic cable with 24 outputs (take out) spaced 5 meters apart, 24 vertical geophones (Natural frequency 10 Hz), A power supply (12V battery), a hammer (10 Kgs) and a metal plate. **(b)** SUMMIT X STREAM Pro Seismograph (DMT): To this we must add; A laptop computer, A digital camera, A navigation GPS and an all-terrain vehicle.

The overall acquisition program (seismic surface tomography) centered on the south portal of the tunnel has been established. It has six lines, three of which are oriented North-South, which are each composed of a seismic profile; while the other three lines are oriented West-East, of which the southernmost line is composed of a single seismic profile and the other two are composed of two seismic profiles each. The two seismic profiles are overlapped on twelve geophones. All the seismic profiles are composed of a seismic base of:

- 24 vertical geophones for recording compression waves,
- 13 shooting points according to the nomenclature presented in the acquisition diagram below,
- 05 shooting points at 30 m offset were made for lines L5 and L6.

The acquisition diagram for the seismic tomography showing the distribution of the geophones and the shot points, is given in the figure (7).

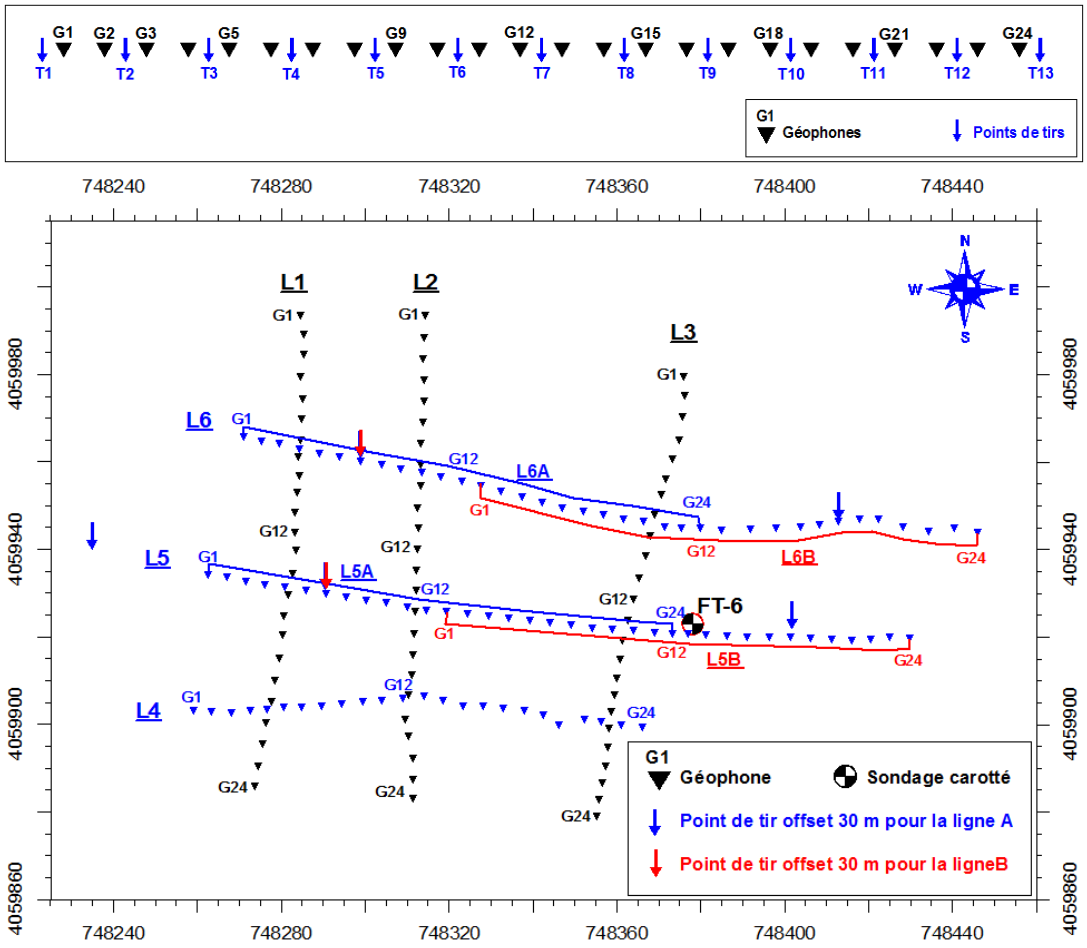

Figure 7: Layout plan for seismic lines at the south portal of the Texanna tunnel.

3.1 METHODOLOGY OF DIFFERENT PROSPECTION TECHNIQUES

3.1.1 Seismic prospecting

The principle of the seismic method consists in causing a shaking which gives rise to a vibratory wave which propagates in all directions, then in recording, via geophones, the arrival of certain waves (compression, shear, etc.) at different stations. The study of the propagation times of the waves makes it possible to define the nature and the geometry of the layers based on the fact that the waves propagate at different speeds in different formations [54]. Among these waves (figure 8), we distinguish a direct wave which propagates on the surface of the ground with the speed of the first terrain (V1) and a refracted wave which propagates at the interface between the first terrain and the underlying one with the speed of the second terrain (V2) in the case where (V2) is greater than (V1).

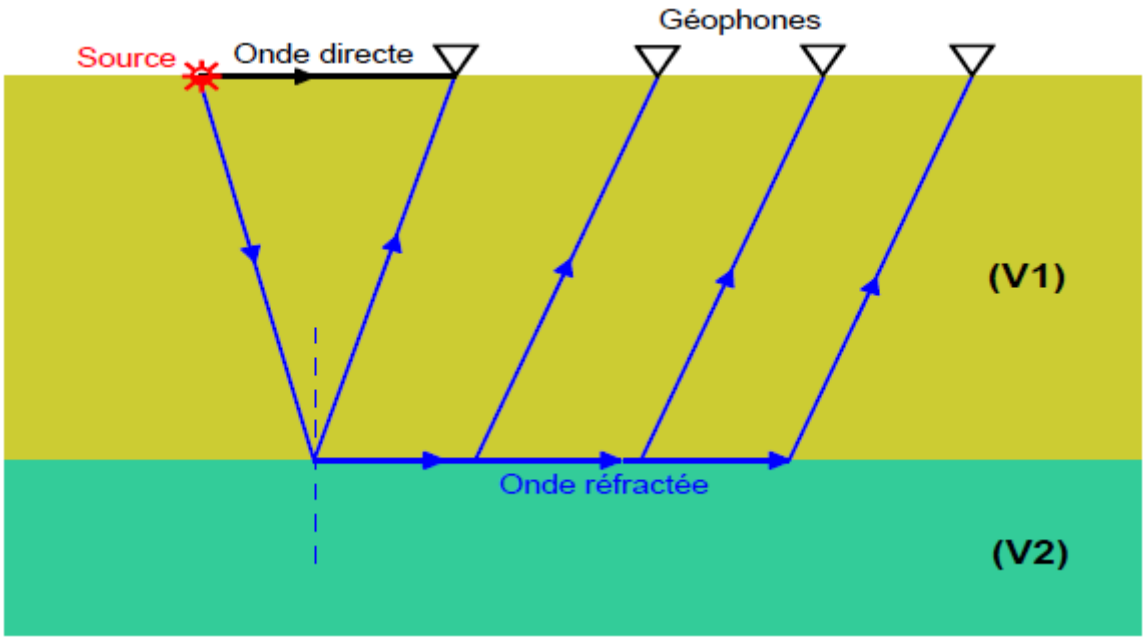

Figure 8: Principle of seismic refraction.

3.1.2 Seismic tomography:

Seismic tomography is widely used for the detection of significant heterogeneities between wells. It also allows, by measurements between galleries, the obtaining of valuable information on the mechanical properties of land in mining and civil engineering. Seismic tomography exploits the propagation of elastic waves to characterize the medium by parameters related to the theory of

elasticity such as the propagation speed of seismic waves [55-57]. The measurement of the travel times of the seismic rays crossing the medium gives the possibility of obtaining the distribution of the velocity parameter in the portion of the prospected subsoil [58-62]. No matter the type of wave treated, we use the analogy with geometric optics and we then consider the wave rays (or spokes) which represent the perpendiculars to the wave fronts. Unlike wave fronts, rays have no physical reality but their use is judicious. Thanks to this technique, the speeds are evaluated, in a grid divided into cells, from the analysis of the times of the first arrivals of the seismic waves which propagate between the transmitter and the receivers. The problem to be solved in seismic tomography is the restitution of the slowness distribution (inverse of the speed) of the longitudinal seismic waves (P) in a medium, from the measurements of the times of arrival observed between sources and receivers of known positions. We call propagation time inversion the determination of the velocity distribution from the measurement data. Different methods have been developed for several years [63-64], we distinguish the matrix inversion methods which are reliable and the geometric inversion methods, generally iterative and which in case of convergence lead to good quality results.

3.2 Geoseismic sections

The interpretation of the results is carried out based on the velocity ranges obtained by inversion. The attributions of these physical parameters to the nature of the geological formations are carried out on the basis of a single log of the core drilling (FT-06) which is available in our study area. This core drilling is located near the LB5 seismic line, between geophones 13 and 14. This positioning was done considering the coordinates in the survey log.

3.2.1 North-South geoseismic sections:

3.2.1 a Surface Seismic Tomography Line L1:

The L1 geoseismic section is located on the western part of the site with a relatively N-S orientation. The velocity model obtained by inversion for this profile has a very acceptable RMS of 1.02 ms. Seismic tomography section L1 (figure 9-a), highlights a relatively tabular ground with seven ranges of speeds which increase according to the depth, which are as follows;

- The first range corresponding to the surface layer is obtained with a speed between 300 and 500 m/s. It is present in a discontinuous way and is attributed to very altered silty clays.
- The second speed range is between 500 and 1000 m/s, it is present along the profile and it is flush between geophones 7 and 13. This speed range is obtained with a variable thickness which can reach 4 meters. It is attributed to silty clays and very hard sandstone blocks.
- The third speed range is between 1000 and 2000 m/s, it is present along the profile with a variable thickness which is very thin on the SE side of the profile. It is attributed to clays and gravelly clays.
- Under this last formation, the speed range between 2000 and 3000 m/s is highlighted with a thickness of about ten meters on the NW side of the profile and which narrows on the SE side. It can be attributed to the formation of very hard clay and sandstone.
- The fifth range of speed, varying between 3000 and 4000 m/s, is located at a depth of 15 meters on the NW side, while on the SE side it rises until reaching a depth of 5 m. At this point it has a maximum thickness of about twenty meters. This velocity range can be attributed to the formation of slightly weathered argillite (clay-stone).
- The last two ranges between 4000 and 5000 m/s are attributed to the formation of argillite (clay-stone) which becomes harder and harder at depth.

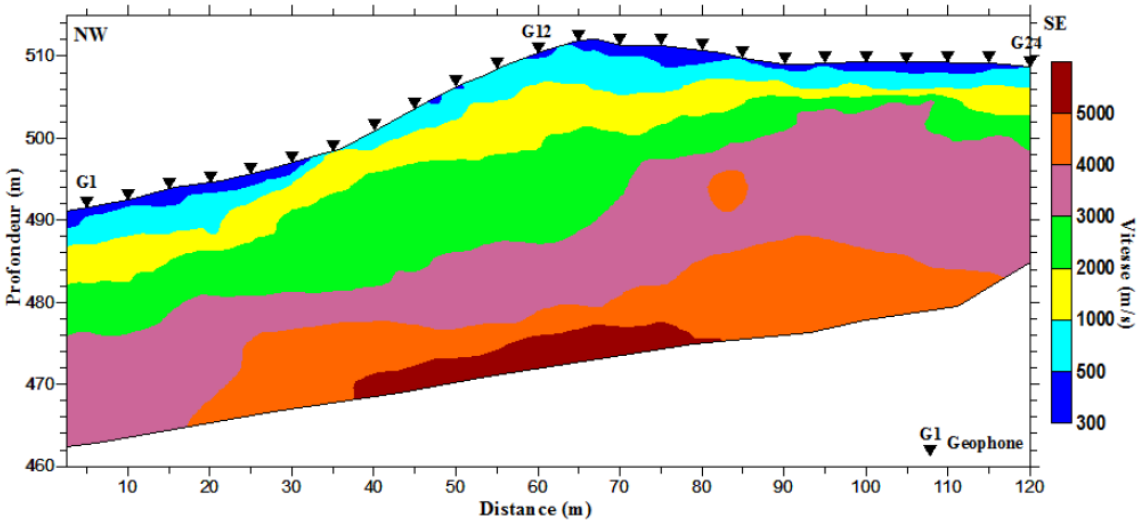

Figure 9: (a) Seismic tomography profile 1 (L1).

3.2.1 b Surface Seismic Tomography Line L2:

The velocity model obtained by inversion for the L2 profile has a very acceptable RMS of 0.98 ms. The section of the seismic tomography line L2 (figure 9-b), is of relatively NW-SE orientation and shows on the whole the same configuration as the previous line, six ranges of speeds which evolve according to the depth, which are as follows;

- The first range corresponding to the surface layer is obtained with a speed between 300 and 500 m/s. It is present throughout the site, except at three points which are located between geophones 9–10, 21 and 23. This velocity range is attributed to highly altered silty clays.
- The second velocity range is between 500 and 1000 m/s, it is present along the profile and it is flush between geophones 9–10, 21 and 23. This speed range is obtained with a thickness that varies between 1 and 6 meters and is attributed to silty clays and very hard sandstone blocks.
- The third range of speed is between 1000 and 2000 m/s, it is present along the profile with a thickness that varies between 2 and 8 meters. This speed range is assigned to clays and gravelly clays.
- The fourth range of speed, between 2000 and 3000 m/s, is highlighted all along the profile with a thickness between 4 and 12 meters. It can be attributed to the formation of very hard clay and sandstone.
- The fifth range of speed, between 3000 and 4000 m/s, can be attributed to the formation of slightly weathered argillite (clay-stone). The roof of this formation has a somewhat bumpy topography.
- The last speed range greater than 4000 m/s is attributed to the formation of hard argillite (clay-stone), is present in the form of a lens located at a depth of about twenty meters between geophones 8 and 14.

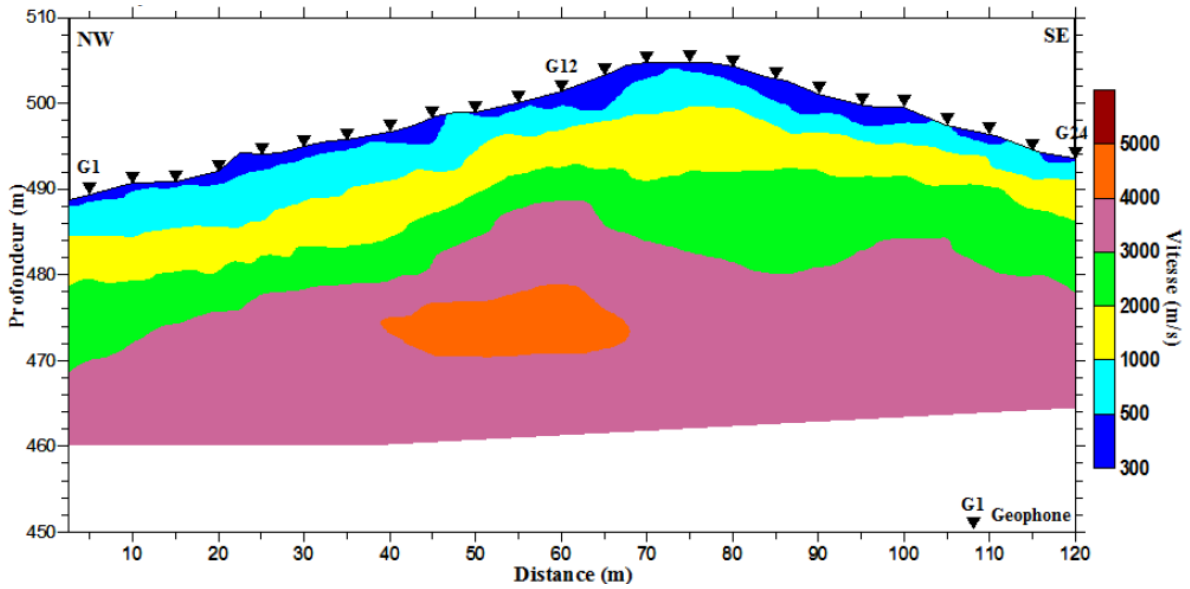

Figure 9: (b) Seismic tomography profile 2 (L2).

3.2.1 c Surface Seismic Tomography Line L3:

The velocity model obtained by inversion for this profile has a very acceptable RMS of 0.89 ms. The L3 geoseismic section is located on the eastern part of the site, with a relatively NW-SE orientation (figure 7). It highlights a relatively tabular terrain with five ranges of speeds that increase with depth, which are as follows;

- The first range corresponding to the surface layer is obtained with a speed between 300 and 500 m/s and an average thickness of 1.5 m. It is present in a discontinuous way, is strongly localized in the center and at the NW end of the profile. This speed range is attributed to highly weathered silty clays.
- The second speed range is between 500 and 1000 m/s, it is present along the profile and it is flush with the surface at several points (figure 9-c) and it disappears on the SE part of the profile. This speed range is obtained with a thickness varying between 1 and 5 meters. It is attributed to silty clays and very hard sandstone blocks.
- The third speed range is between 1000 and 2000 m/s, it is present along the profile with a variable thickness which is very thin on the SE side of the profile at the level of the talweg. It outcrops on the surface at the SE end of the profile, is attributed to clays and gravelly clays.
- Under this last formation, the speed range between 2000 and 3000 m/s is highlighted with a significant thickness on the NW side and which narrows

on the SE side, at the level of the thalweg, to reach 1 m. It can be attributed to the formation of very hard clay and sandstone.

- The last range of speed greater than 3000 m/s is located at variable depths between 2 m, at the level of the taweg, and exceeds 30 m and plunges in depth on the NW side of the profile. This velocity range can be attributed to the formation of slightly weathered argillite (clay-stone).

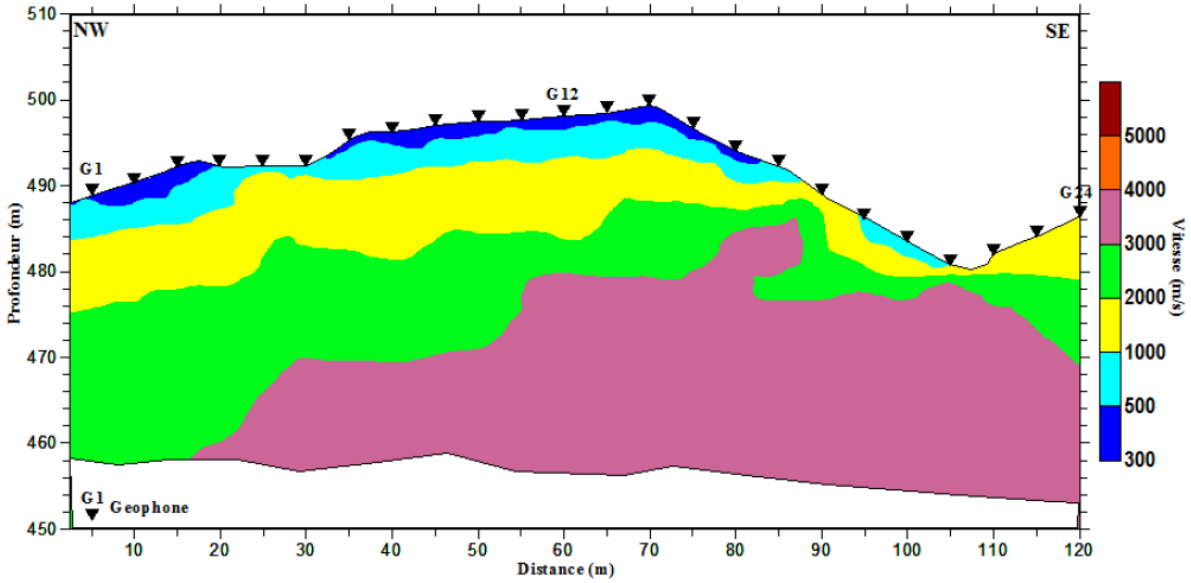

Figure 9: (c) Seismic tomography profile 3 (L3).

3.2.2 West-East geoseismic sections

3.2.2 a Surface Seismic Tomography Line L4:

The velocity model obtained by inversion for the L4 profile has an acceptable RMS of 1.38 ms. The section of the L4 seismic tomography profile located in the southernmost part of the study area (Figure 7), is oriented W-E and shows the same velocity configuration as the previous profiles. Seven speed ranges are highlighted and show an increase in speed with depth, which are as follows;

- The first range corresponding to the surface layer is obtained with a speed between 300 and 500 m/s and an average thickness of 1.5 m. It is present in a discontinuous way, and it disappears on the east side of the profile. This speed range is attributed to highly weathered silty clays.
- The second range of speed is between 500 and 1000 m/s, it is present in a continuous way and which is flush with the surface on several points (figure 10-a) and it disappears on the eastern part of the profile. This speed range is

obtained with a thickness that varies little around 2 meters. It is attributed to silty clays and very hard sandstone blocks.

- The third range of speed is between 1000 and 2000 m/s, which is attributed to clays and gravelly clays, it is present along the profile with a thickness between 1.5 and 6 m. It is flush on the surface at the east end of the profile.
- The formation that can be attributed to very hard clays and sandstones is obtained with a range of speed between 2000 and 3000 m/s that is highlighted with a thickness varying from 1 to 8 m.
- The fifth speed range between 3000 and 4000 m/s is highlighted with a strong thickness on 3/4 of the profile on the east side of the profile. However, on the 1/4 of the remaining profile on the west side, this thickness is around 2 m. This velocity range can be attributed to the formation of slightly weathered argillite (clay-stone).
- The speed range above 4000 m/s is attributed to the formation of argillite (clay-stone) which becomes increasingly hard at depth. This formation is highlighted in the form of two lenses: the first is located at the start of the profile between geophones 1 and 9 and where this clay-stone becomes harder and harder at depth; the second is present directly above geophones 15 and 21.

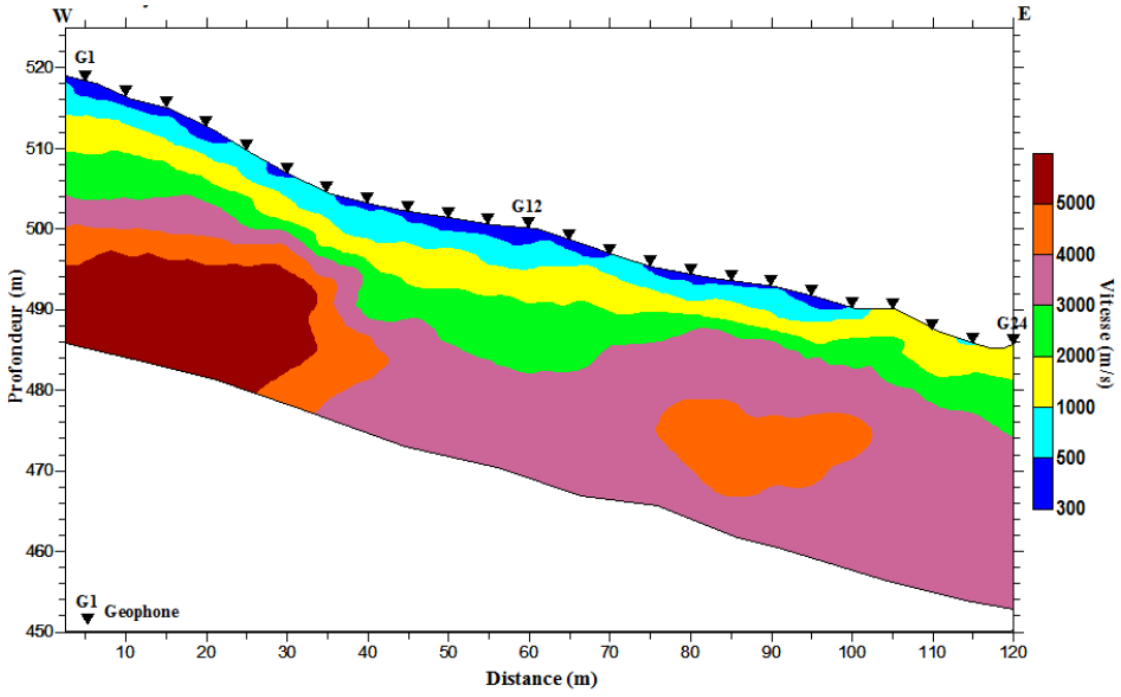

Figure 10: (a) Seismic tomography profile 4 (L4).

3.2.2 b Surface Seismic Tomography Line L5:

This line is composed by two profiles which cover a length of 180 m. It is intersected by the FT-6 cored borehole between geophones 25 and 26 (figure 7). The velocity model obtained by inversion for the L5 profile has an acceptable RMS of 1.05 ms. The L5 seismic tomography section (Figure 10-b), is oriented W-E and shows tabular layers that correlate relatively well with the thicknesses of the FT-6 core drilling. These layers are obtained with seven ranges of speeds evolving according to the depth which are as follows;

- The first range corresponding to the surface layer is obtained with a speed between 300 and 500 m/s, the maximum thickness of which does not exceed two meters. This layer is present in a discontinuous way and is attributed to very altered silty clays.
- The second speed range is between 500 and 1000 m/s, it is present along the profile and it is flush with the surface in places, especially on the east side of the profile. This speed range is obtained with a variable thickness between 2 and 8 meters. It is attributed to silty clays with gravel and pebbles and very hard sandstone blocks.
- The speed range between 1000 and 2000 m/s is attributed to clays and gravelly clays, its thickness varies between 2 and 10 m.
- The fourth range of speed varying between 2000 and 3000 m/s represents according to the FT-6 survey, an alternation between clays and very hard sandstones with a passage of silty sand.
- The fifth range of speed between 3000 and 4000 m/s is highlighted relatively on the whole of the profile, and which plunges in depth in the center of the profile. This velocity range can be attributed to the formation of slightly weathered argillite (clay-stone).
- The last two ranges of speeds varying between 4000 and 5000 m/s are attributed to the formation of argillite (clay-stone) which becomes harder and harder at depth.

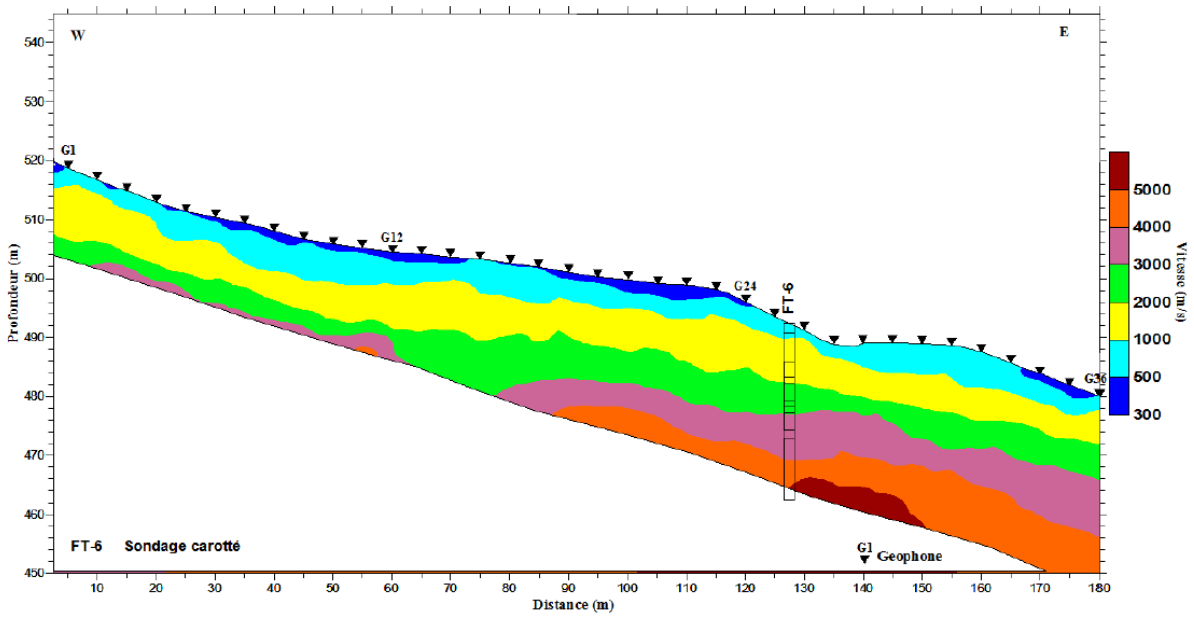

Figure 10: (b) Seismic tomography profile 5 (L5).

3.2.2 c Surface Seismic Tomography Line L6:

The velocity model obtained by inversion for the L6 profile has an acceptable RMS of 1.30 ms. The section of the L6 seismic tomography profile located in the northernmost part of the study area (Figure 7), is oriented W-E and shows the same velocity configuration as the previous profiles. Seven speed ranges are highlighted and show an increase in speed with depth, which are as follows;

- The first range corresponding to the surface layer is obtained with a speed between 300 and 500 m/s and with a thickness varying between 0.5 and 3 m. It is present in a discontinuous way, and it disappears at both ends of the profile. This speed range is attributed to highly weathered silty clays.
- The second range of speed is between 500 and 1000 m/s, it is present in a continuous way and which is flush with the surface on several points (figure 10-c) and it disappears on the extreme eastern part of the profile. This speed range is obtained with a slightly variable thickness which is between 1 and 6 meters. It is attributed to silty clays and very hard sandstone blocks.
- The third range of speed is between 1000 and 2000 m/s, which is attributed to clays and gravelly clays, it is present along the profile with a thickness between 2 and 10 m. It is flush on the surface at the east end of the profile.

- The formation that can be attributed to very hard clays and sandstones, is obtained with a range of speed between 2000 and 3000 m/s is highlighted with a variable geometry, whose thicknesses vary from 2 to about fifteen meters and it dives deep on the east side of the profile. This formation is intersected by a more compact formation (higher velocity) between geophones 4 and 9.
- The fifth range of speed between 3000 and 4000 m/s is highlighted on the whole of the profile and plunges in depth at the East end of the profile. This range of velocity can be attributed to the formation of slightly weathered argillite (clay-stone). The thickness of this formation varies from 1 to about twenty meters.
- Under the slightly weathered argillite formation, we find the velocity range above 4000 m/s, which is attributed to the argillite (clay-stone) formation which becomes harder and harder at depth. This formation is highlighted between the second and twenty-sixth geophone.

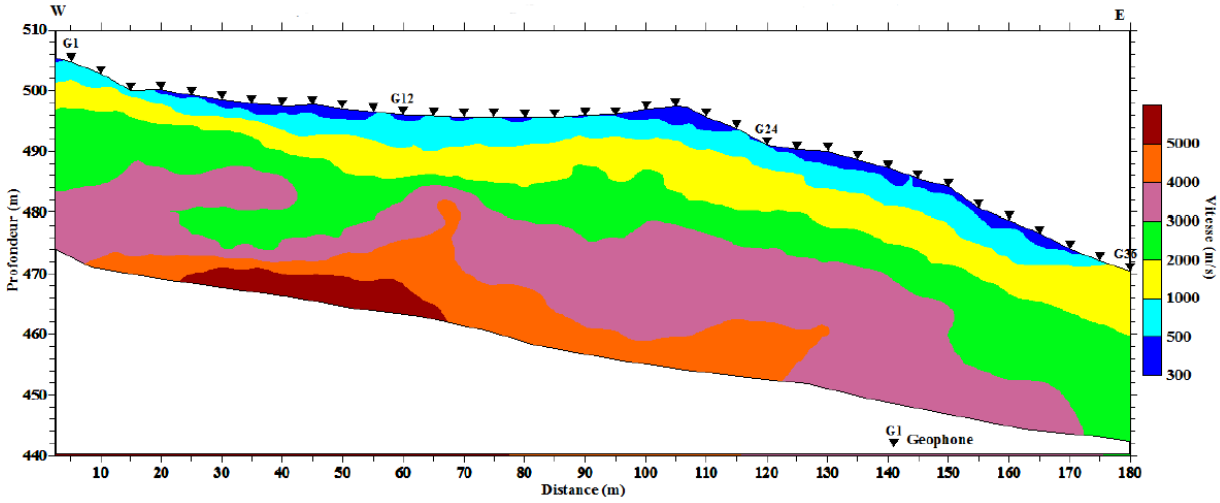

Figure 10: (c) Seismic tomography profile 6 (L6).

4 NUMERICAL COLLAPSE ANALYSIS OF THE SOUTH PORTAL SLOPE

Because the height of the total slope of the south portal of the tunnel is between 45 and 65 meters, they are of high importance. Therefore in the south portals of the tunnel, it was made the collapse analyzes by the program Phase 2D

V.8.0. In the analyses, the value of critical SRF (strength reduction factor) we determined. This analyses are done separately for the cases of unsupported, supported and with the earthquake and the stability of the portal has been evaluated. The main reason for using the phase program since the environment is the rock and the supported systems that can be used in detail. The modelling which was used for the analysis follows the geological units which are presented on the model (figure 11-a).

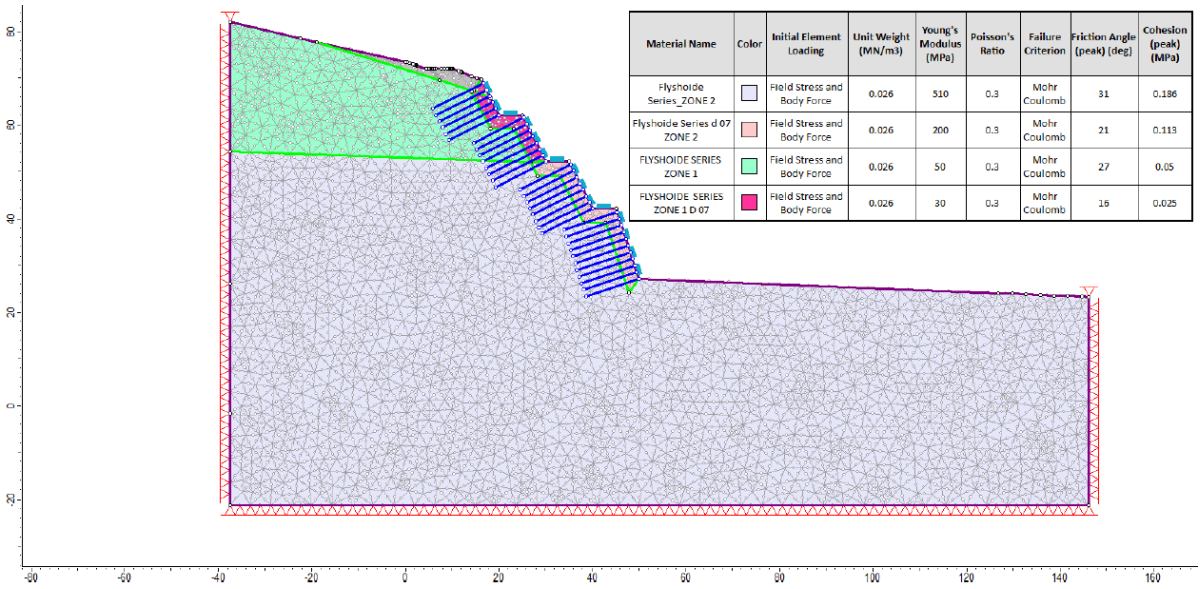

Figure 11: (a) The model formed and geological units by Phase 2D program.

In the south portal of the tunnel, because of the most critical height of the section is 45 meters, the analyses are done for slopes inclined. The models that are used in the analyses are shown in Figure (11-a) above. The results of the analyses are shown in Figures (11-b, 11-c and 11-d). At the unsupported situation the value of SRF is (strength reduction factor) found as 0.91. Because of the value of SRF is less than 1.5 and the height of the slope is about 55 meters, analyses are repeated for the situation supported. Considering the situation with support, the analyses were repeated for bolts 12 m long and a pattern of 2 x 2 m, for the last two slopes at the bottom. For other slopes, analyses were repeated for bolts 12 m long, a pattern of 1.5 x 1.5 m, with a diameter of 32 mm, shotcrete thickness of 15 cm, and two wire mesh (steel lattice). According to the results of the analyses the value of SRF is calculated as 1.6. In the case of an earthquake, the value of SRF was obtained as 1.33, considering the time when the excavation of the slopes of the portal was completed and just before the construction of the covered trench.

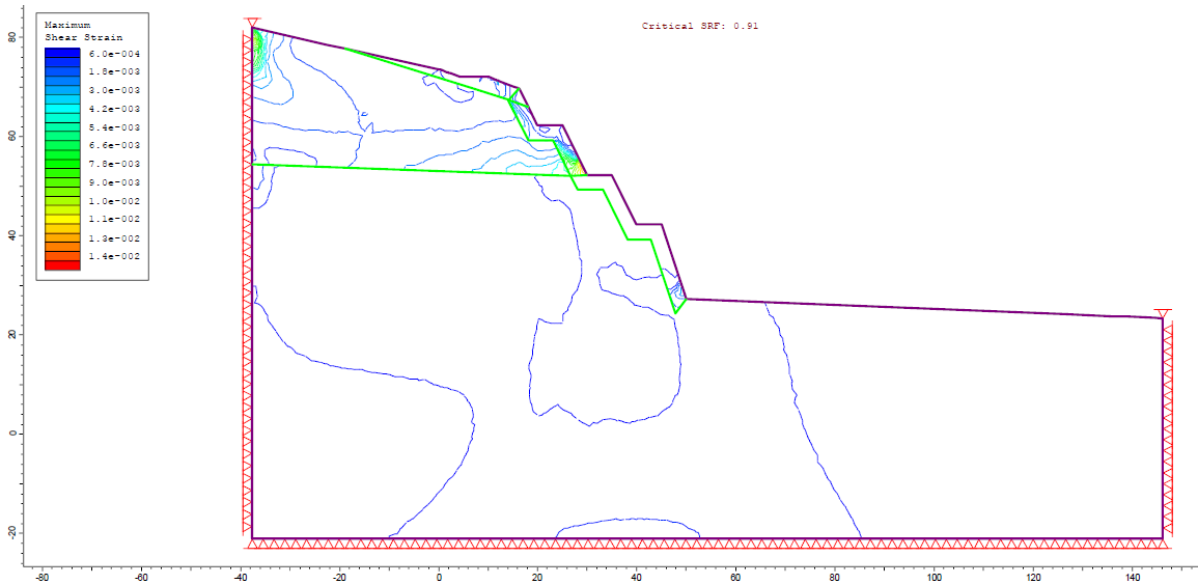

Figure 11: (b) The results of the analyzes made in non-supported situation, SRF=0,91.

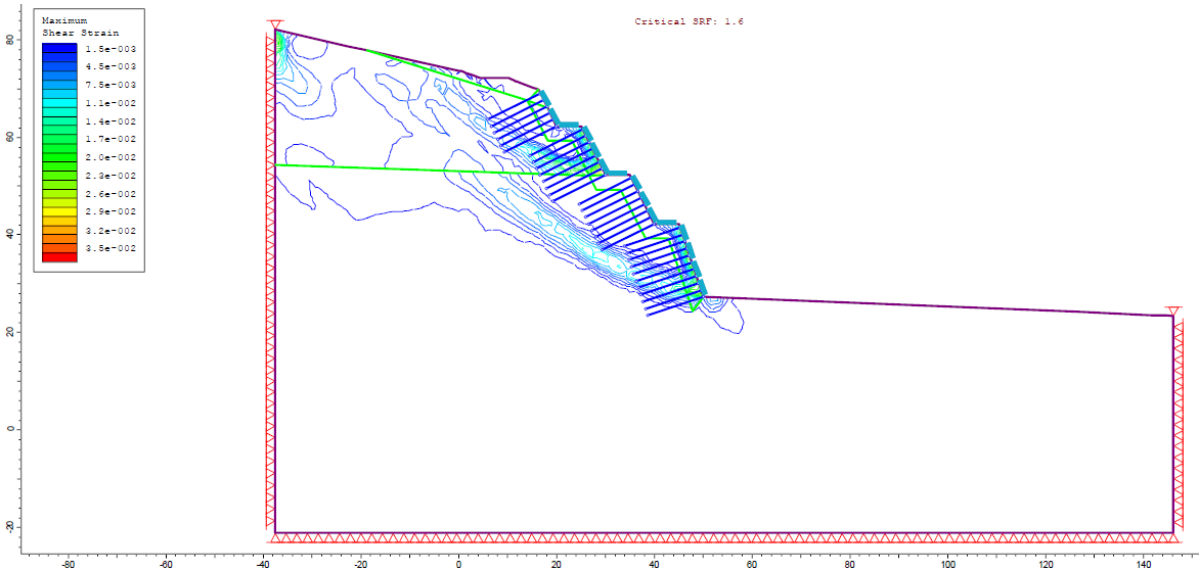

Figure 11: (c) The results of the analyzes in supported situation, SRF=1.5.

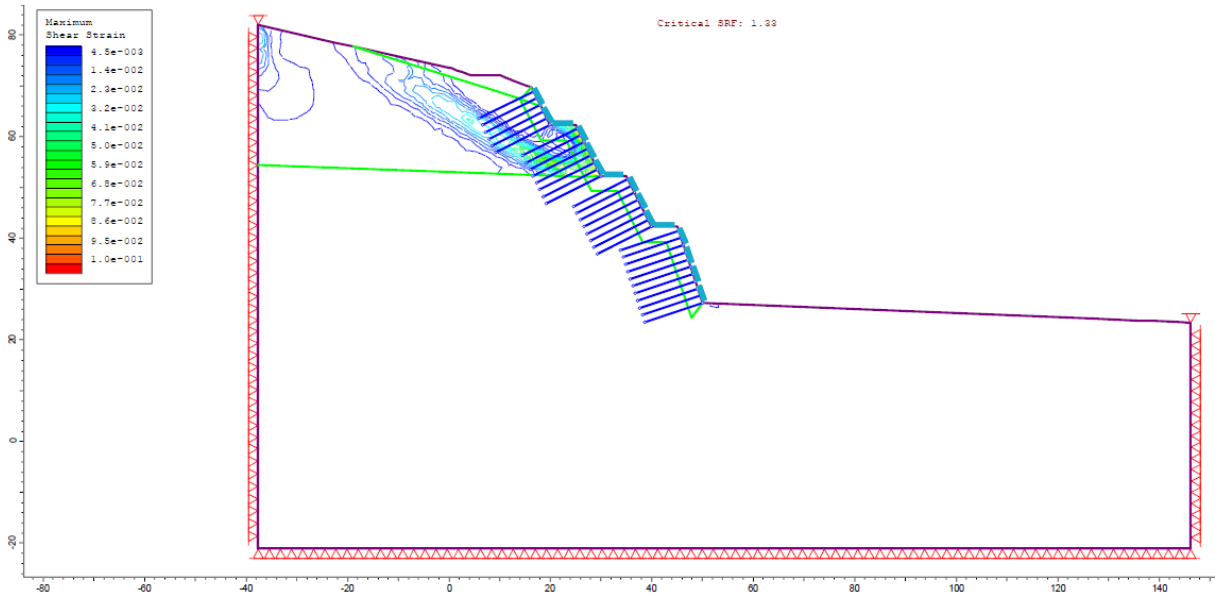

Figure 11: (d) The results of analyzes done in supported situation and with an earthquake, SRF=1.33

5 APPLICATION OF THE SUPPORT SYSTEM TO THE PORTALS SLOPES

Based on the analyses above, rock bolts 32 mm in diameter, 12 m in length and 1.5x1.5 m in size (pattern) are recommended on the slope surfaces of the tunnel entrance portal (figure 12 and table 1). Stability is ensured in the slope surfaces of the front of the exit portal with rock bolts 32 mm in diameter, 12 m in length and 2x2 m in size on the surface of the first two (2) lower slopes and 12 m in length and 1.5x1.5 m on the surfaces of the slopes that follow. In addition, anchoring bolts of 12 m length in 2x2 pattern are recommended for the 2 lower right lateral slopes of the exit gate and 12 m in model length 1.5 x 1.5 m, 32 mm diameter for other upper slopes. In addition to the south portal the entire surface of the slope of 15 cm thick type C30 / 37 with shotcrete, two wicker steel ply was recommended. The diameter of the forge will be 76 mm. In this part of the portal, because of the absence of massive rocks and solid ground, Swellex anchor bolts are not possible to drive in. Swellex anchor bolts are recommended in areas where there is solid rock and where there is water flow. For the drainage of groundwater and surface water in the slope of the portal, the pits of the head, palya and heel have been proposed. In addition, barbican it must be applied on the surface of the

slope. The parameters that will be applied to weep holes (barbicans) should be adjusted by the anchor bolt pattern. As a result, in the slope surfaces with a model 1.5 x1.5 and 2x2 and the length of 12 meter and 32 mm diameter anchor bolt, the model of barbican should be 3x3 and 4x4 m and 12 meter in length. By taking approval on the administration, to avoid clogging of the joints by thin drifting materials, it must be packed the perforated PVC with felt. Perforated PVC pipes will be used 2 "in diameter and wrapped by geotextile and 12 m in length, it will be produced as the perforated upper half. Typical failure potential of overthrow (overturning) will be avoided by bolts of 12 m in length that will be driven to the surface of the slope.

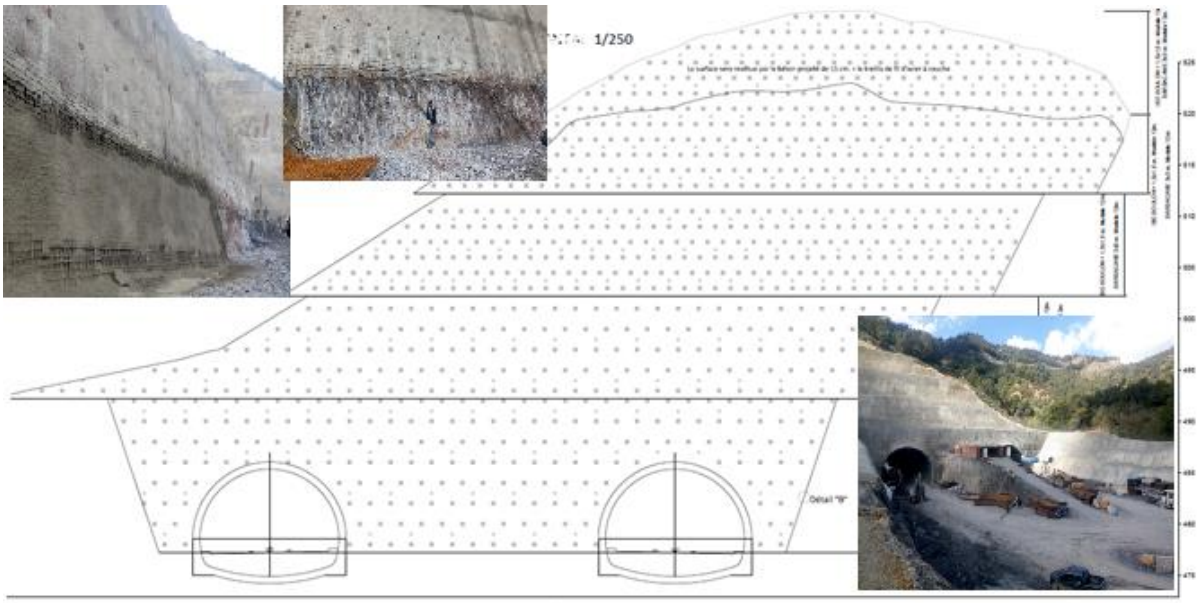

Figure 12 (a): Location section view of the front end bolt system 1/250.

The slope geometry taken for all the slopes of the entrance portal (figure 12-b) is 1H:3V. In the exit portal;

- for the first slope under the slopes of the front we take 1H:3V, and 1H:2V for the following upper slopes of the front,
- for the first slope under the right side slopes we take 1H:3V, and 1H:2V for the following upper right side slopes,
- For the left side slope we take 1H:1V.

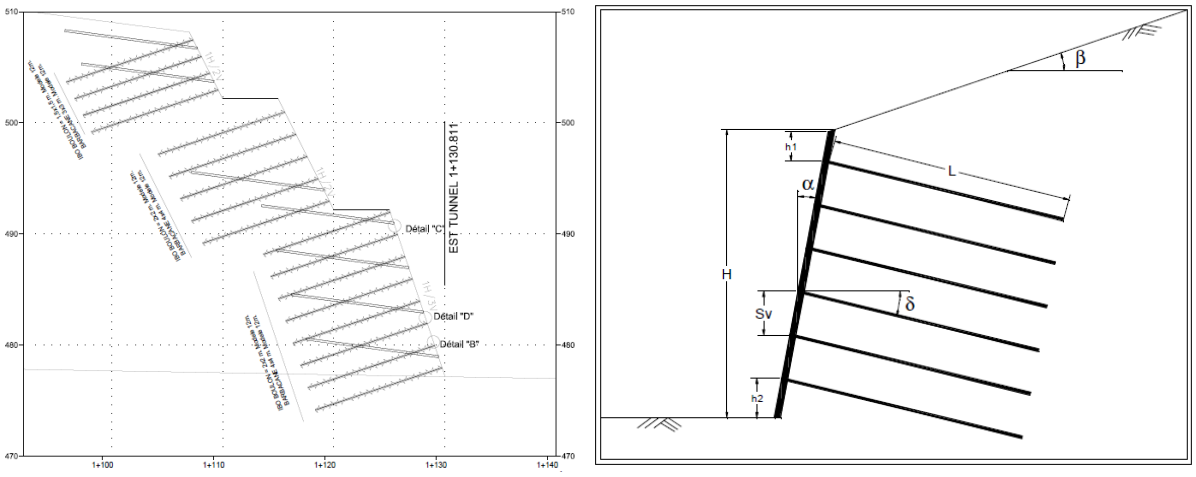

(b) (c)

Figure 12: (b): View bolt system localization section of the east tube 1/250, (c) Croquet of anchoring angle of anchor bolts [65,66].

The locations of the portal anchor bolts are as follows:

- ✓ Notes;
  - Excavations will be done in layers of 2m,
  - The retaining/ supporting systems will be installed after each layer excavation. The excavation of the next layer will be started only after the installation of the supports.
  - A controlled explosion will be applied if necessary in the geological conditions encountered during the excavation.
  - The support methods will be revised according to the geological conditions encountered during the excavation.
  - It is impossible in this type of soil to ensure the stability of open wells for bolts of 12 m length to be implanted in the section of the gate. In addition, it is impossible to install the 12m bolts in the case of SN or PG bolts. As a result, all bolts to be implanted must be self-drilling bolts (IBO).
  - Geological mapping will be carried out during the excavations of the gates and the retaining systems will be revised according to the new conditions.
- ✓ Materials;
  - Bolt: ST III,
  - Welded steel mesh: ST IV,
  - steel shoring: ST 37,
  - Shotcrete: RN 30.
- ✓ Bolt pull test;
  - At least one test bolt will be designed for each row of bolts,
  - Test bolts will not be project bolts,

- The test will be carried out by means of pull test the loading layers will be: 0.5, 10, 16, 10, 5, 0.10, 16, 20, 25, 10 tons,
- We will wait at least 10 minutes in the loading layers (except unloading) and readings will be made at minutes 0, 1, 2, 3, 4, 5 and 10. In case of persistent deformations, the readings will be redone in the 15th, 25th, 30th, 45th and 60th minutes.
- In case of collapse before reaching a load of 16 tons, the bolt size must be revised.
-

Table 1: Geometries & Characteristics.

Cutting geometry		
(H)	Cutting height	15,00 m
(α)	Angle of the slope with the vertical plane	72°
(β)	Ground angle of the slope surface with the horizontal plane	5°
Design Geometry		
(δ)	Angle of the nail with the horizontal plane	15°
(Sv)	Vertical nail spacing	1,50 m
(Sh)	Horizontal nail spacing	1,50 m
(D)	Nail hole diameter	0,076 m
Characteristics		
(Fy)	Nail flow stress under tension	420 MN/m²
(f'c)	Pressure resistance of shotcrete	30 MN/m²
(f'i)	Injection pressure resistance	20 MN/m²

6 MONITORING OF THE SOUTH-PORTAL DISPLACEMENTS

To observe the stability of the slope of the portal in the long term, it is suggested to open 19 reference points (PR) divided into four (04) different levels slopes on the south portal of the tunnel. There will be 4 to 5 reference points on each slope. The deepest points above the portal level limit (-40 m) are PR1, PR2, PR3, PR4 and PR5. Then, the points above by 15 meter (-25m) are PR 6, PR 7, PR 8, PR 9 and PR 10. Then, the points above by 10 meter (-15m) are PR 11, PR12, PR13, PR14 and PR15. Finally, the most superficial points of the slope below the ground by 5 meters (-05m) are PR16, PR17, PR18 and PR19. In addition, the reference points (PR) plan recommended in the South portal is presented below (figure 13).

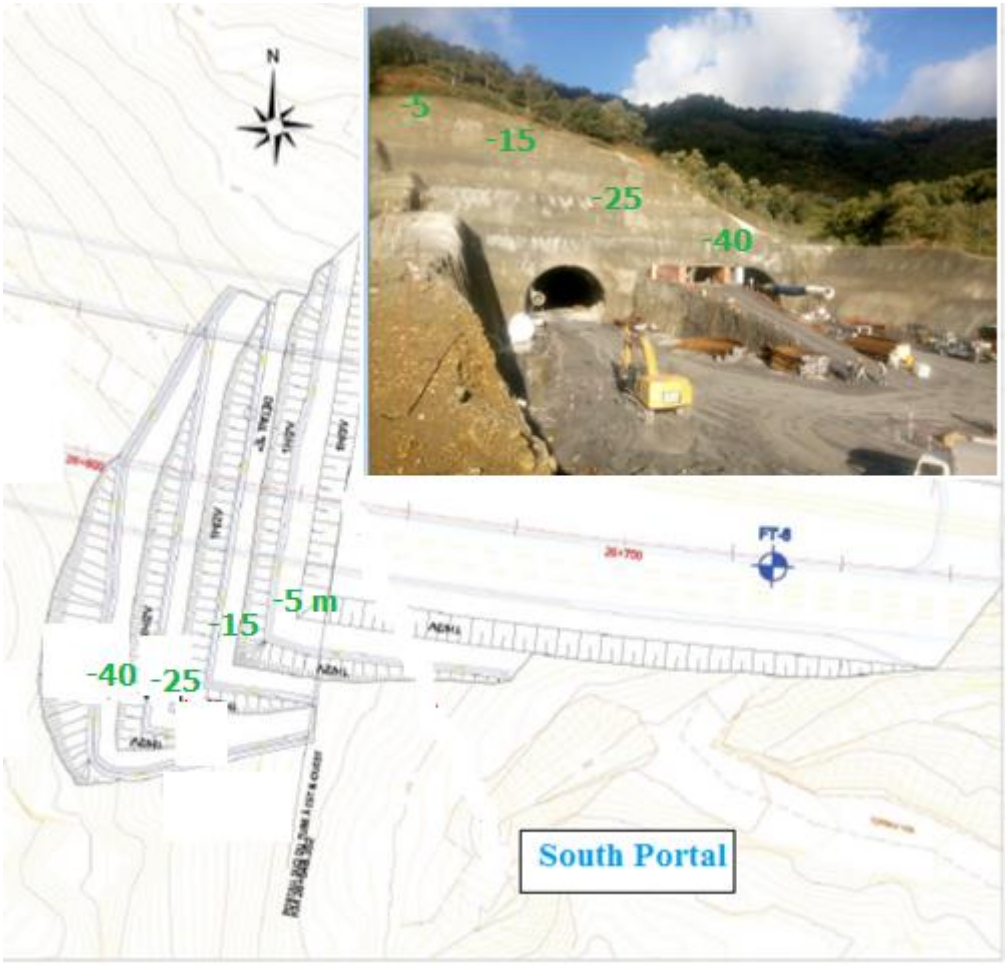

Figure 13: Sounding installation plan located on the South Portal section for portal deformation measurements.

For a period of about 300 days; it was observed in the first upper level (-5m) of the south portal slope (figure 14) a total settlement of 5 mm at point P16, 22 mm at point P17, 40 mm at point P18 and 8 mm at point P19, A total East-West displacement of 0 mm at point P16, 24 mm at point P17, 26 mm at point P18 and 3 mm at point P19 and a total North-South displacement of 6 mm at point P16, 26 mm at point P17, 11 mm at point P18 and 20 mm at point P19. Also, it can be noted that the deformation did not start until the beginning of May 2017 and continues to gradually increase then begins to straighten almost linearly until it reaches its maximum in the points (P17, P18 and P19) and it can be considered almost punctual in point P16.

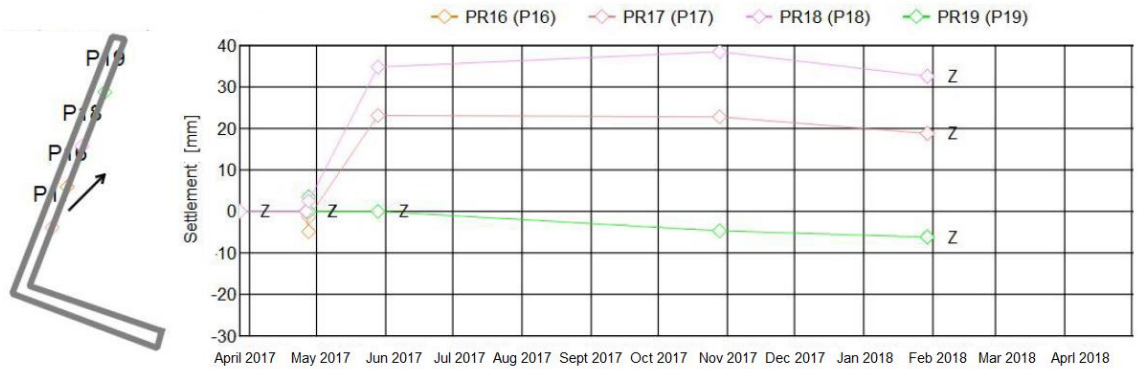

(a) settlement (mm)

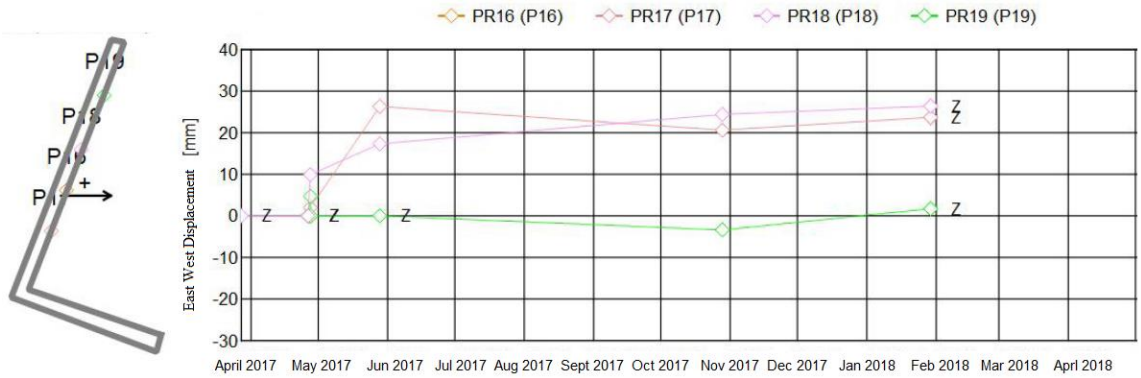

(b) East West Displacement

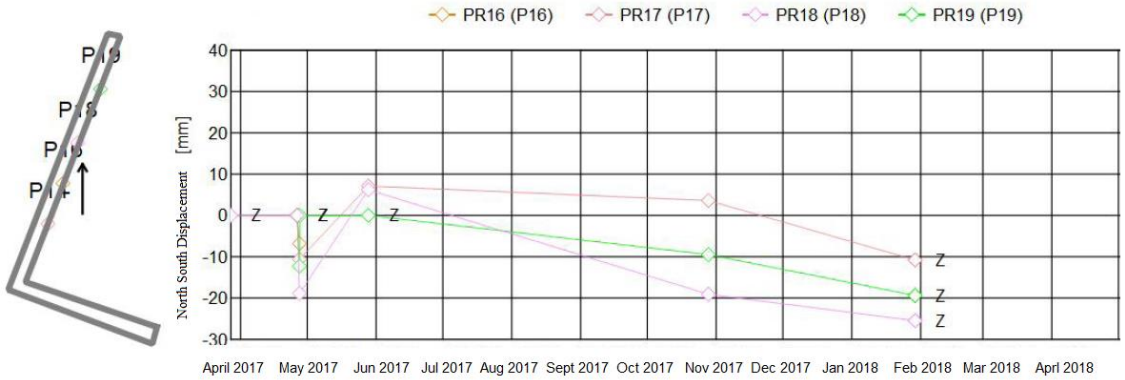

(c) North South Displacement

Figure 14: Displacement diagrams - Cross section: -5,000. First measurement: 27.03.2017. Last measurement: 29.01.2018.

Afterwards, in the second level below the previous one (-15m) of the south portal slope (figure 15) for a period of approximately 398days, it was observed a total settlement of 30mm at point P11, 02mm at point P12, 38mm at point P13, 36mm at point P14 and 40mm at point P15. A total East-West displacement of 30mm at point P11, 18mm at point P12, 27mm at point P13, 34mm at point P14 and 20mm at point P15. A total North-South displacement of 54mm at point P11,

34 mm at point P12, 26 mm at point P13, 40 mm at point P14 and 27 mm at point P15. Also, it can be noted that most of the deformations start to appear in March 2017 and then stabilize in May 2017 and they can be considered irregular deformations in all measured points.

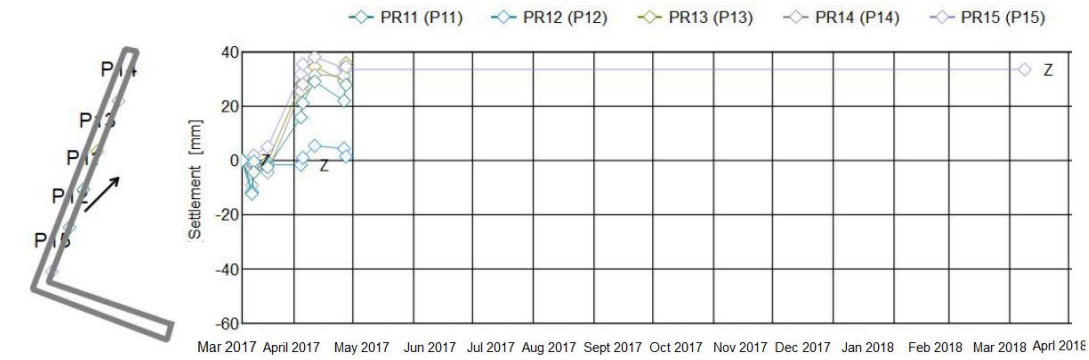

(a) settlement (mm)

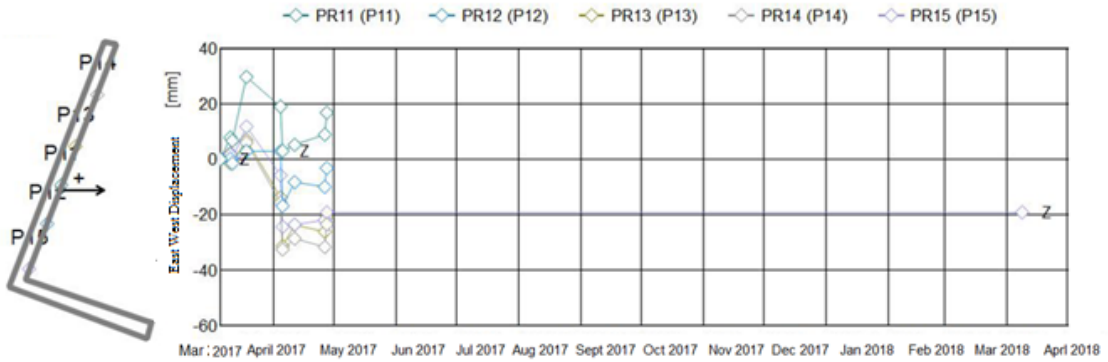

(b) East West Displacement

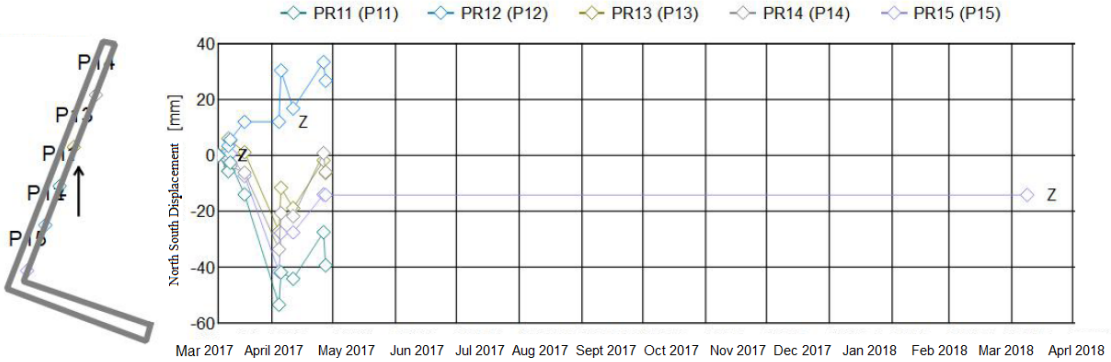

(c) North South Displacement

Figure 15: Displacement diagram - Cross section: -15,000. First measurement: 05.03.2017. Last measurement: 08.04.2018.

Afterwards, in the third level below the previous one (-25 m) of the south portal slope (figure 16) for a period of approximately 403 days, it was observed a total settlement of 78 mm at point P6, 22 mm at point P7, 24 mm at point P8, 60 mm at point P9 and 80 mm at point P10. A total East-West displacement of 11

mm at point P6, 38 mm at point P7, 38 mm at point P8, 22 mm at point P9 and 2 mm at point P10. A total North-South displacement of 79 mm at point P6, 64 mm at point P7, 66 mm at point P8, 44 mm at point P9 and 38 mm at point P10. Also, it can be noted that the deformation started at the beginning of January 2017 and it continues to increase gradually, then it begins to recover in an almost linear manner until reaching its maximum in all the measurement points.

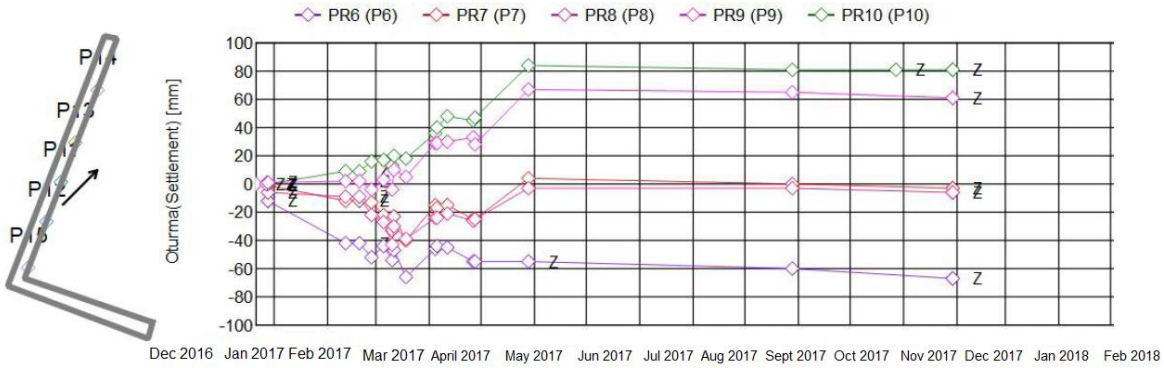

(a) settlement (mm)

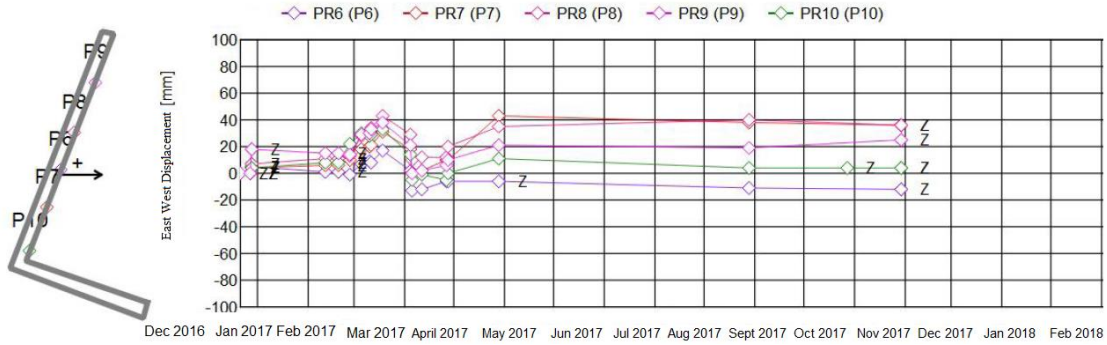

(b) East West Displacement

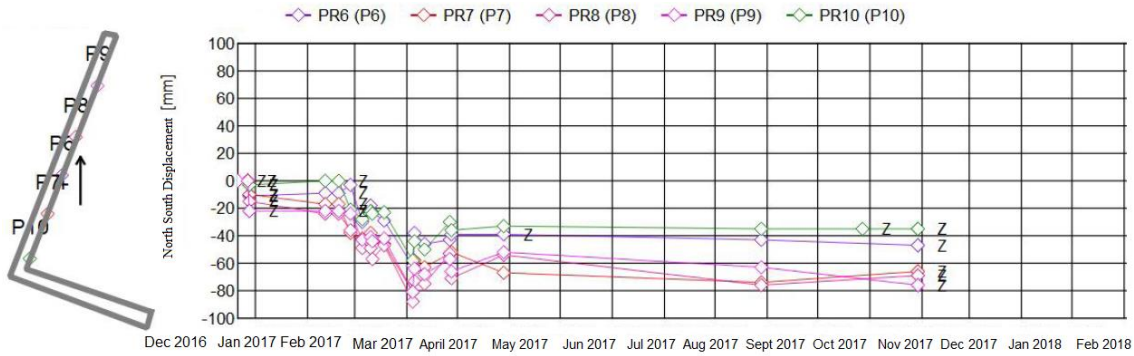

(c) North South Displacement

Figure 16: Displacement diagram - Cross section: -25,000. First measurement: 21.12.2016. Last measurement: 29.01.2018.

Finally, in the fourth level below the previous one (-40 m) of the south portal slope (figure 17) for a period of about 403 days, it was observed a total settlement of 88 mm at point P1, 79 mm at point P2, 79 mm at point P3, 60 mm at point P4 and 39 mm at point P5. A total East-West displacement of 10 mm at point P1, 00 mm at point P2, 00 mm at point P3, 39 mm at point P4 and 70 mm at point P5. A total North-South displacement of 24 mm at point P1, 24 mm at point P2, 24 mm at point P3, 84 mm at point P4 and 70 mm at point P5. Also, it can be noted that most anomalies start to appear in January 2017 with irregular behavior in all points then they start at the equator linearly from May 2017.

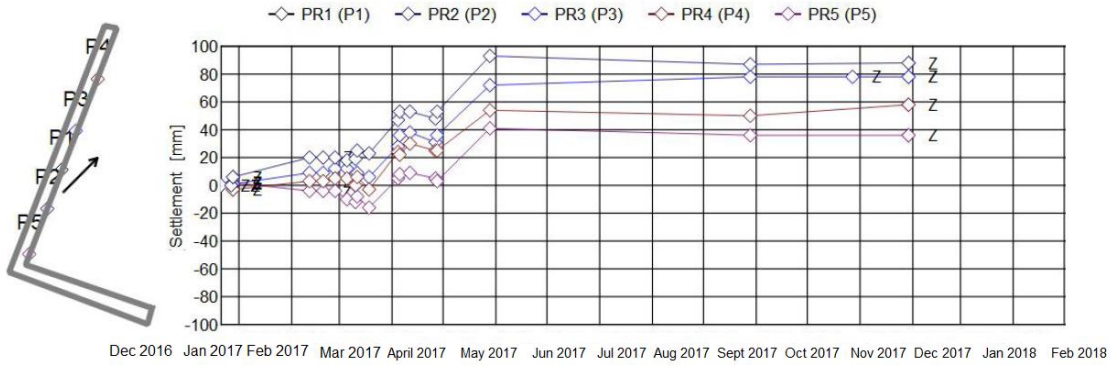

(a) settlement (mm)

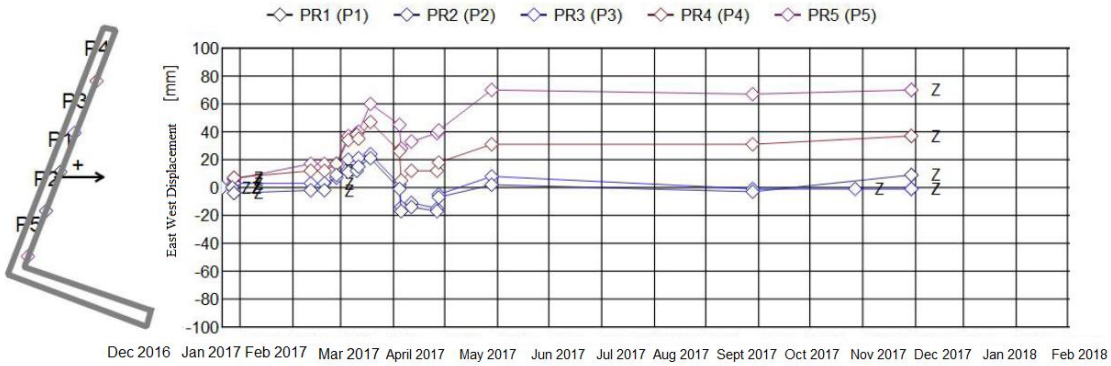

(b) East West Displacement

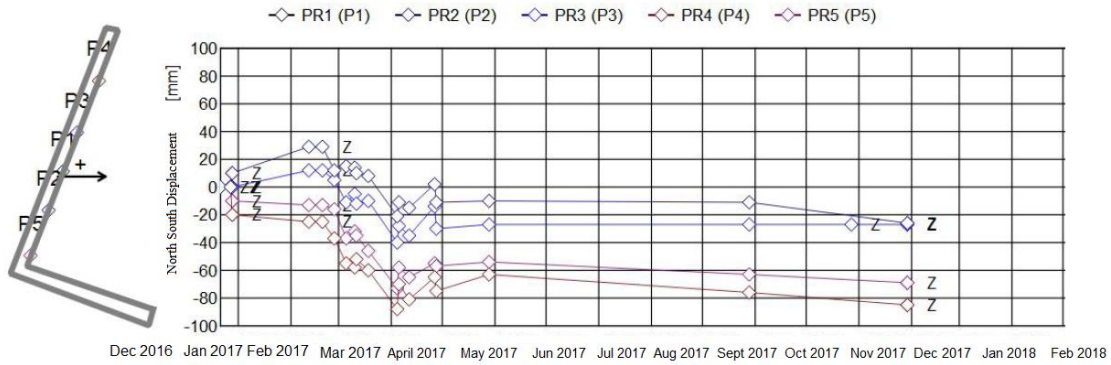

(c) North South Displacement

Figure 17: Displacement diagram - Cross section: -40,000. First measurement: 21.12.2016. Last measurement: 29.01.2018.

We can summarize the maximum deformations for each depth above the tunnel portal in figure (18). What is remarkable is that the settlements increase as the depth increases; this is very logical because the further we get from the tunnel boundary, is the less rock mass movement there is due to confinement. Also; we can notice that the north-south displacements are bigger than the east-west displacements except in the first level of the slope; this is probably due to the characteristics of the rock mass and to the influence of the steps and drilling locations inside the tunnel. At the end, we can conclude that the deformations at the slope of the south portal of the tunnel are acceptable, and they do not represent any danger or threat compared to the numerical analysis above (figure 11).

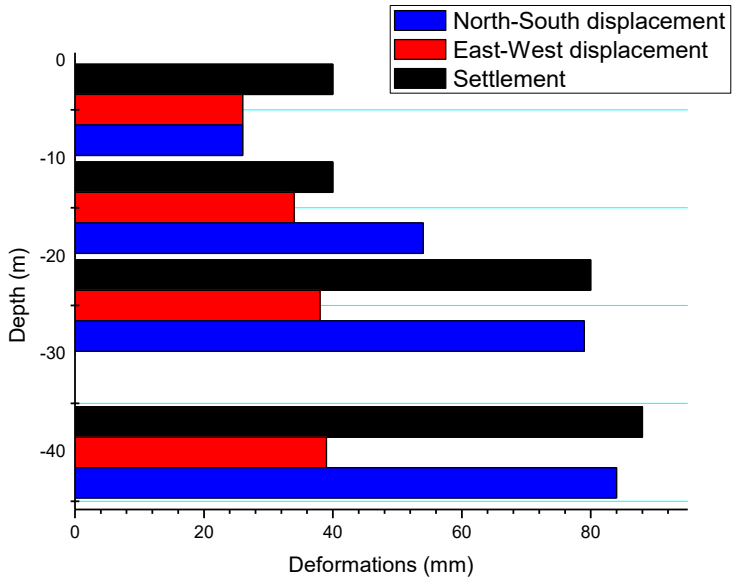

Figure 18: Maximum deformations diagram in each level and different directions of the south portal slope.

7 CONCLUSION

This article was written to determine the slope stability of the south portal by the anchor bolt support system of the Texana twin-tube tunnel in Jijel province, in Algeria. According to survey data and fieldwork, there is a flysch unit which consisted of thin-medium stratified mudstone, medium-thick stratified intercalated sandstone, aged Albo-Aptian. In order to meet the needs of the study, a geophysical prospecting was carried out at the level of the South portal of the Texana tunnel project by the surface seismic tomography method, with the aim of determining;

- the lithology of the different formations and their geometry,
- the variation in speed of the subsurface formations at the south portal of the Texana tunnel.

The analysis of the results of seismic tomography made it possible to reach certain conclusions on the geometric configuration of the terrains. The interpretation of the results was carried out based on the velocity ranges obtained by inversion and on the attributions of these physical parameters to the nature of the geological formations are carried out on the basis of the log of the core drilling (FT-6) which is available in our study area. The profiles made at the level of the south portal on the Texana tunnel project have made it possible to highlight seven distinct speed ranges and show an increase in speed as a function of depth, namely;

- The first range corresponding to the surface layer is obtained with a speed between 300 and 500 m/s. It is present discontinuously. This speed range is attributed to highly weathered silty clays.
- The second range of speed is between 500 and 1000 m/s, it is present in a continuous manner and it is flush with the surface in certain places. It is attributed to silty clays and very hard sandstone blocks.
- The third range of speed is between 1000 and 2000 m/s, it is flush with the surface in places and it can be attributed to clays and gravelly clays.
- The formation that can be attributed to very hard clays and sandstones, is obtained with a range of speed between 2000 and 3000 m/s.
- The fifth range of speed between 3000 and 4000 m/s can be attributed to the formation of slightly weathered argillite (clay-stone).
- The last speed range above 4000 m/s is attributed to the formation of argillite which becomes increasingly hard at depth. This formation is highlighted, in places in the form of two lenses.

The portal excavation and tunnels opened with the sandblasting method as they knew that this situation will be a serious impact on the portal. With the effect of sandblasting the discontinuity clearance is increased and new openings can occur. It is impossible in this type of soil to ensure the stability of the open pits for the 12 m long bolts to be implanted in the portal section. Also, it is not possible to install the 12m bolts in case they are SN or PG bolts. Consequently, all bolts to be implanted must be self-drilling bolts (IBO). Therefore, the stability of the portal will be affected negatively, after sandblasting the properties of the rock

mass can be changed in a negative direction. With the supported systems available, stability issues that may occur in the future will be avoided.

Acknowledgements

This work is under the auspices of the General Directorate of Scientific Research and Technological Development (DGRSDT) of the Algerian Ministry of Higher Education and Scientific Research (MESRS).

REFERENCES

[1] Goricki W, Schubert G, Riedmueller G. New developments for the design and construction of tunnels in complex rock masses. International Journal of Rock Mechanics and Mining Sciences 2004;41(3):497-8.

[2] H. Khelalfa, June 2020. Tunnel Executors- NATM's Recommendations and Guidelines. LAMBERT Academic Publishing. ISBN: 978-620-2-67199-6.

[3] Schubert W. Basics and application of the austrian guideline for the geomechanical design of underground structures. In: EUROCK2004 and 53th Geomechanics Colloquium. VGE; 2004.

[4] Potsch M, Schubert W, Goricki A, Steidl A. Determination of rock mass behaviour types, a case study. In: EUROCK2004 and 53th Geomechanics Colloquium. VGE; 2004.

[5] Palmstrom A, Stille H. Ground behaviour and rock engineering tools for underground excavations. Tunnelling and Underground Space Technology 2007;22(4):363-76.

[6] Taromi M, Eftekhari A, Hamidi JK, Eghbali A (2018) Tunnel designing and construction process in difficult ground conditions using controlled deformations (ADECO) approach; a case study. Int J Min Geo-Eng IJMGE 52–2:149–160

[7] Sun S, Li S, Li L, Shi S, Wang J, Hu J, Hu C (2019) Slope stability analysis and protection measures in bridge and tunnel engineering: a practical case study from Southwestern China. Bull Eng Geol Environ 78:3305–3321

[8] ROUILI, A., TOUAHMIA, M. and DJERBIB, Youcef (2018). Numerical analysis of the partial collapse of a twin-tubes tunnel. In: KOHOUTKOVA, Alena, VITEK, Jan L.,FRANTOVA, Michaela and BILY, Petr, (eds.) Proceedings of the 12th international PhD symposium in civil engineering. federation internationale du beton (fib), 641-648.

[9] Messioud S, Mokhbi H, Khelalfa H, Khelalef, Ishaq Laouar. Collapse Investigation and Numerical analysis of the Repair and completion of the Twin-Tube Tunnel of Jebel El-

Ouahch T1 in Constantine Province, Algeria. *Indian Journal of Engineering*, 2021, 18(50), 240-257

[10] Fang Q, Zhang D, Li Q, Ngai L, Wong Y. Effects of twin tunnels construction beneath existing shield-driven twin tunnels. Tunnelling and Underground Space Technology 2015;45:128-37.

[11] Osman AS. Stability of unlined twin tunnels in undrained clay. Tunnelling and Underground Space Technology 2010;25(3):290-6.

[12] Soliman E, Duddeck H, Ahrens H. Two- and three-dimensional analysis of closely spaced double-tube tunnels. Tunnelling and Underground Space Technology 1993;8(1):13-8.

[13] Sahoo JP, Kumar J. Stability of long unsupported twin circular tunnels in soils. Tunnelling and Underground Space Technology 2013;38:326-35.

[14] Zhang ZX, Liu C, Huang X, Kwok CY, Teng L. Three-dimensional finite-element analysis on ground responses during twin-tunnel construction using the URUP method. Tunnelling and Underground Space Technology 2016b;58: 133-46.

[15] Mirsepahi, M., Nayeri, A., Lajevardi, S.H. *et al.* Effect of multi-faced twin tunneling in different depths on a single pile. *Innov. Infrastruct. Solut.* **6,** 42 (2021). https://doi.org/10.1007/s41062-020-00425-5

[16] Kaya A, Akgu¨n A, Karaman K, Bulut F (2016) Understanding the mechanism of slope failure on a nearby highway tunnel route by different slope stability analysis methods: a case from NE Turkey. Bull Eng Geol Environ 75:945–958

[17] Aygar EB, Gokceoglu C (2020) Problems encountered during a railway tunnel excavation in squeezing and swelling materials and possible engineering measures: a case study from Turkey. Sustainability 12:1166

[18] Alija S, Torrijo FJ, Quinta-Ferreira M (2014) Study of the unexpected collapse of Ampurdan tunnel (Spain) using finite element model. Bull Eng Geol Environ 73(2):451–463. https://doi.org/10.1007/s10064-013-0534-z

[19] Jiading Wang, Youjiang Zeng, Yuanjun Xu & Kaiqiang Feng (2017) Analysis of the influence of tunnel portal section construction on slope stability, Geology, Ecology, and Landscapes, 1:1, 56-65, DOI: 10.1080/24749508.2017.1301062

[20] Cao, L. H., & Lu, Z. L. (2013). Tunnel entrance slope stability analysis. Foreign Highway, 04, 244–246.

[21] Wang, F. (2013). The construction technology of shallow buried bias tunnel hole entrance section. Shanxi Architecture, 39, 152–153.

[22] Wang X, Chen J, Zhang Y, Xiao M (2019) Seismic responses and damage mechanisms of the structure in the portal section of a hydraulic tunnel in rock. Soil Dyn Earthq Eng 123:205–216

[23] Rao K, Singh T (2017) Two-dimensional finite element based parametric analysis of South portal slope, Rohtang Tunnel, India. Proc Eng 173:1330–1333

[24] Kaya A, Karaman K, Bulut F (2017) Geotechnical investigations and remediation design for failure of tunnel portal section: a case study in northern Turkey. J Mount Sci 14(6):1140–1160

[25] Genis¸ M (2010) Assessment of the dynamic stability of the portals of the Dorukhan tunnel using numerical analysis. Int J Rock Mech Min Sci 47:1231–1241

[26] Khan RMA, Mad Z, Jo B (2019) Tunnel portal construction using sequential excavation method: a case study, MATEC web of conferences 138, 04002 (2017) EACEF 2017. Acta Polytech 59(5):435–447

[27] Farhad Farhadi Ayoubloua, Majid Taromib and Abbas Eftekharic. TUNNEL PORTAL INSTABILITY IN LANDSLIDE AREA AND REMEDIAL SOLUTION: A CASE STUDY. Acta Polytechnica 59(5):435–447, 2019. DOI:10.14311/AP.2019.59.0435

[28] Emad, M.Z., Khan, M.U., Raza, M.A. et al. Optimum Design of Half Tunnels for Transportation in the Himalayas. Transp. Infrastruct. Geotech. (2021). https://doi.org/10.1007/s40515-021-00162-x

[29] Panji M, Koohsari H, Adampira M, Alielahi H, Marnani JA. Stability analysis of shallow tunnels subjected to eccentric loads by a boundary element method. Journal of Rock Mechanics and Geotechnical Engineering 2016;8(4):480-8.

[30] Addenbrooke T, Potts DM. Static response of reinforced soil retaining walls with nonuniform reinforcement. International Journal of Geomechanics 2001;1(2): 249-71.

[31] Houssam KHELALFA, Nabile OSMANE, Mohammed BOUATIA. Excavation Stability Study with Inclination of Cut Slopes at 45° and 90° in the long-term (LT) and short-term (ST) States: A Case Study. Indian Journal of Engineering, 2020, 17(48), 470-482

[32] Chehade FH, Shahrour I. Numerical analysis of the interaction between twintunnels: influence of the relative position and construction procedure. Tunnelling and Underground Space Technology 2008;23(2):210e4.

[33] Zhang ZX, Xu Y, Kulatilake PHSW, Huang X. Physical model test and numerical analysis on the behavior of stratified rock masses during underground excavation. International Journal of Rock Mechanics and Mining Sciences 2012;49: 134-47.

[34] Sylvanus Sebbeh-Newton, Shaib Abdulazeez Shehu, Prosper Ayawah, Azupuri A. Kaba & Hareyani Zabidi | (2021) Analytical and numerical assessment of a preliminary support design – a case study, Cogent Engineering, 8:1, 1869367, DOI: 10.1080/23311916.2020.1869367

[35] Peng, S. J., Ma, Y., Wang, J. D., & Xie, W. L. (2013). Application of fuzzy information optimization technology on analysis of loess landslide stability. Applied Mechanics and Materials, 321–324, 2389–2395.

[36] Yoo C (2009) Performance of multi-faced tunnelling–A 3D numerical investigation. Tunn Undergr Space Technol 24(5):562–573. https ://doi.org/10.1016/j.tust.2009.02.005

[37] Karakus M, Fowell RJ (2006) 2-D and 3-D finite element analyses for the settlement due to soft ground tunnelling. Tunn Undergr Space Technol 21(3):392–392

[38] A. Ghadimi Chermahini & H. Tahghighi (2019) Numerical finite element analysis of underground tunnel crossing an active reverse fault: a case study on the Sabzkouh segmental tunnel, Geomechanics and Geoengineering, 14:3, 155-166, DOI: 10.1080/17486025.2019.1573323

[39] Chu B, Lin Y. Mechanical behavior of a twin-tunnel in multi-layered formations. Tunnelling and Underground Space Technology 2007;22(3):351e62.

[40] Zheng G, Du Y, Cheng X, Diao Y, Deng X, Wang F (2017) Characteristics and prediction methods for tunnel deformations induced by excavations. Geomech Eng 12(3):361–397

[41] Ou CY, Hsieh PG (2011) A simplified method for predicting ground settlement profiles induced by excavation in soft clay. Comput Geotech 38(8):987–997

[42] Terzaghi K, Peck RB. Soil mechanics engineering practice. John Wiley; 1948.

[43] Peck RB. Advantages and limitations of the observational method in applied soil mechanics. Géotechnique 1969;19(2):171-87.

[44] Spross J, Johansson F. When is the observational method in geotechnical engineering favorable? Structural Safety 2017;66:17e26.

[45] Sakurai S, Akutagawa S, Takeuchi K, Shinji M, Shimizu N. Back analysis for tunnel engineering as a modern observational method. Tunnelling and Underground Space Technology 2003;18(2e3):185-96.

[46] Chapman T, Green G. Observational method looks set to cut city building costs. Proceedings of the Institution of Civil Engineers e Civil Engineering 2004;157(3):125-33.

[47] Finno RJ, Calvello M. Supported excavations: observational method and inverse modeling. Journal of Geotechnical and Geoenvironmental Engineering 2005;131(7):826-36.

[48] Fuentes R, Pillai A, Ferreira P. Lessons learnt from a deep excavation for future application using the observational method. Journal of Rock Mechanics and Geotechnical Engineering 2018;10(3):468-85.

[49] Glass PR, Powderham AJ. Application of the observational method at the limehouse link. Géotechnique 1994;44(4):665-79.

[50] Peck RB. The observational method can be simple. Proceedings of the Institution of Civil Engineers e Geotechnical Engineering 2001;149(2):71-4.

[51] L Joleaud; M Ferrand; E Ficheur; Algeria. S Carte géologique de l'Algérie 1:50,000. 74, El Aria. ervice de la carte géologique de l'Algérie., 1908.

[52] Wildi, W. (1983) La chaine tello-rifaine (Algérie, Maroc, Tunisie): Structure, Strati-Graphie et évolution du Trias au Miocène. Revue de Géologie dynamique et de Géographie Physique, 24, 201-297

[53] Hamou Djellit, Évolution tectono-métamorphique du socle Kabyle et polarité de mise en place des nappes de flysch en petite Kabylie occidentale (Algérie), Supported in 1987 at Paris 11 university, in partnership with University of Paris-Sud. Faculty of Sciences of Orsay (Essonne).

[54] Alhussein A. Basheer, Khamis Q. Mansour & Mohammed A. Abdalla (2014) Geophysical investigation to reveal the groundwater condition at new Borg El-Arab industrial city, Egypt, NRIAG Journal of Astronomy and Geophysics, 3:2, 117-129, DOI: 10.1016/j.nrjag.2014.08.002

[55] C. A. Moreira, M. M. Lapola & Alan Carrara. 2016. Comparative analyzes among electrical resistivity tomography arrays in the characterization of flow structure in free aquifer. Geofísica internacional 55 no.2 México abr./jun.2016 versión impresa.

[56] C. C. Okpoli. 2013. Sensitivity and Resolution Capacity of Electrode Configurations. Department of Geology and Applied Geophysics, Faculty of Science, Adekunle Ajasin University, PMB 001, Akungba-Akoko,Ondo State, Nigeria. Hindawi Publishing Corporation International Journal of Geophysics 2013, Article ID 608037, p.3. http://dx.doi.org/10.1155/2013/608037.

[57] Loke, M. H. (1997) Rapid 2D resistivity inversion using the least-squares method RES2DINV Program; Manual: Penang, Malaysia.

[58] McMECHAN, G.A. 1983, Migration by Extrapolation of Time-Dependent Boundary Values, Geophysical Prospecting 31,413-420.

[59] Ivansson S. (1987) Crosshole transmission tomography. In: Nolet G. (eds) Seismic Tomography. Seismology and Exploration Geophysics, vol 5. Springer, Dordrecht. https://doi.org/10.1007/978-94-009-3899-1_7

[60] N. D. Bregman, R. C. Bailey, and C. H. Chapman, (1989), "Crosshole seismic tomography," GEOPHYSICS 54: 200-215

[61] Pratt, R. and Sams, M. (1996). Reconciliation of crosshole seismic velocities with well information in a layered sedimentary environment. Geophysics, 61(2), 549-560. http://dx.doi.org/10.1190/1.1443981

[62] Joe Wong, (2000), "Crosshole seismic imaging for sulfide orebody delineation near Sudbury, Ontario, Canada," GEOPHYSICS 65: 1900-1907. https://doi.org/10.1190/1.1444874

[63] Thurber, C. (2015). Treatise on Geophysics || Theory and Observations - Seismic Tomography and Inverse Methods. , (), 307–337. doi:10.1016/b978-0-444-53802-4.00009-9

[64] Zhao D. (2015) Methodology of Seismic Tomography. In: Multiscale Seismic Tomography. Springer Geophysics. Springer, Tokyo. https://doi.org/10.1007/978-4-431-55360-1_2

[65] FHWA. 1998. Manual for design and construction monitoring of soil nail walls. US Department of Transportation, Washington, D.C. FHWA-SA-96-069R.

[66] A.A.S.H.T.O.2002. «Standard Specifications for Highway Bridges». ISBN: 9781560511496